Dispersion and brightness studies in the Proton Synchrotron Booster

CERN Summer Student: Pittau Giorgia

Summer Student 2024 Report

Supervisors
Foteini Asvesta
Tirsi Prebibaj

October 3, 2024

Contents

1 Introduction

To understand the behavior of particle beams in accelerators, it is essential to first analyze the motion of a single particle within the accelerator. The horizontal position of the single particle is influenced by both betatron oscillations and dispersive effects due to momentum deviation.The particle's horizontal position can be expressed as the sum of the betatron and dispersive components:

$$x = x_b + x_d = x_b + D_x \left(\frac{\delta p}{p}\right) \tag{1.1}$$

where, x_b represents the betatron position, while x_d accounts for the dispersive contribution. The dispersion function, D_x, describes how the position of a particle with a momentum deviation $\delta p/p$ deviates from the nominal trajectory due to the presence of dipole magnets in the beamline, which are required to keep the particle on a circular trajectory. When particles pass through a dipole magnet, their trajectories are bent according to their momentum, leading to a spread in their final positions.
If it is assumed that the betatronic and dispersive positions are independent and that both distributions are Gaussian, considering a set of particles yields:

$$\langle x^2 \rangle = \langle x_b^2 \rangle + \langle x_d^2 \rangle = (\sqrt{\beta_x \varepsilon_{x,\mathrm{RMS}}})^2 + \left[D_x \left(\frac{\delta p}{p}\right)_{\mathrm{RMS}}\right]^2 \tag{1.2}$$

Thus, the total variance in the horizontal plane σ_x is given by the combination of the betatronic and dispersive contributions:

$$\sigma_x^2 = \sigma_b^2 + \sigma_d^2 = \sigma_b^2 + \left[D_x \left(\frac{\delta p}{p}\right)_{\mathrm{RMS}}\right]^2 \tag{1.3}$$

where σ_b is the betatronic beam size, and σ_d is the dispersive contribution.
By rearranging this expression, the horizontal emittance, which is the main quantity of interest in this study, can be derived:

$$\varepsilon_{x,RMS} = \frac{\beta\gamma}{\beta_x} \left[\sigma_x^2 - \left[D_x \left(\frac{\delta p}{p}\right)_{\mathrm{RMS}}\right]^2\right] \tag{1.4}$$

From this expression, it can be observed how the emittance is related to the dispersion D_x. To reconstruct the betatron distribution, the goal is to eliminate or at least reduce the dispersive part. The only way to eliminate this contribution is to achieve a zero dispersion configuration at the measurement point, as the momentum spread cannot be entirely eliminated, only reduced. In practice, the measured distribution is a convolution of the betatron and dispersive components, as shown in Fig.(1.1). The dispersive component follows a parabolic distribution, and what is observed tends to resemble a q-Gaussian distribution (see Appendix A).

2 Dispersive profile measurement and convolution with various q-Gaussian profiles

To understand the connection between the betatron distribution and the measured distribution, the dispersive distribution was convolved with various q-Gaussian distributions, each corresponding to a different possible betatron distribution. The result of this convolution represents the measurement that would be obtained given a specific, unknown initial betatron distribution.

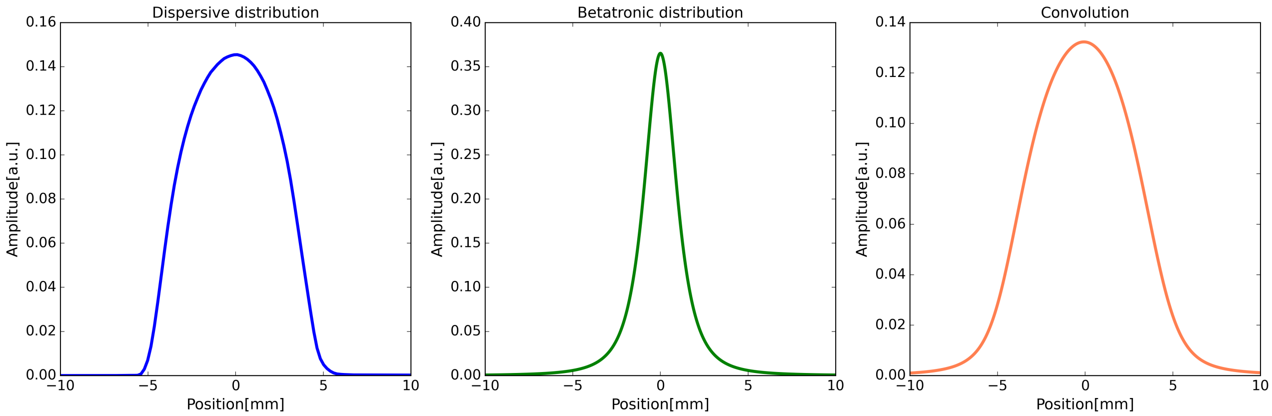

Figure 1.1: Example of dispersive and betatron distributions, along with their convolution.

The dispersive profile was initially measured using a tomoscope at various intensities. As expected, on first order, the profiles did not vary significantly across different intensities; thus, they were averaged to obtain a single profile at a fixed $\delta p/p$. This averaged profile was then utilized in the convolution analysis with q-Gaussian distributions. The fit values obtained from this convolution are shown in the sidebars for q and q-Gaussian σ in Fig.(2.1), respectively. It is important to note that σ_0 and σ_{fit} in these plots represent q-Gaussian values, not Gaussian ones.

A similar plot was generated using the Gaussian σ_0, which was extracted by fitting the generated q-Gaussian distribution with a standard Gaussian, rather than using the σ_0 from the q-Gaussian itself. This mapping is illustrated in Fig.(2.2). The fitting process is shown for the case of a q-Gaussian generated with $q = 1.3$ and $\sigma_q = 1.6$ in Fig.(2.4).

Using the Gaussian σ values for both the betatronic (generated) and convolution distributions, emittance values were derived and presented as a function of emittance rather than σ, as shown in Fig.(2.3). This approach allowed for the creation of a map that facilitates deriving the parameters of the distribution that need to be measured from the parameters of the betatron q-Gaussian distribution.

The betatronic distribution, by definition, follows a q-Gaussian profile. The key conclusion of this analysis is that the tails (q) of the measured, convoluted profile appear smaller than those of the betatronic distribution. This discrepancy is attributed to the parabolic shape of the dispersive component. Consequently, based on these simulations, it is expected that the actual tails in the PSB are larger than what the measurements suggest. In section (4), experimental measurements were conducted to study this behavior.

3 Simulations in *Xsuite* for reducing dispersion in wire scanner and scraper

As previously mentioned, one potential method to reduce and ideally eliminate the dispersive contribution to the position is to achieve a configuration with zero dispersion at the points where measurements are taken or where beam tails are scraped — specifically at the wire scanner and scraper positions. Dispersion control within the machine is primarily managed by adjusting the quadrupoles. In the PSB, there are 16 defocusing quadrupoles powered in series, each with a common strength of k_{brqd}, along with a global corrective trim $k_{brqdcorr}$. Similarly, there are 32 focusing quadrupoles, also powered in series, each with a common strength of k_{brqf} and a global corrective trim $k_{brqfcorr}$. The focusing quadrupoles are half the length of the defocusing quadrupoles. However, the global corrections $k_{brqfcorr}$ and $k_{brqdcorr}$ were not considered in the

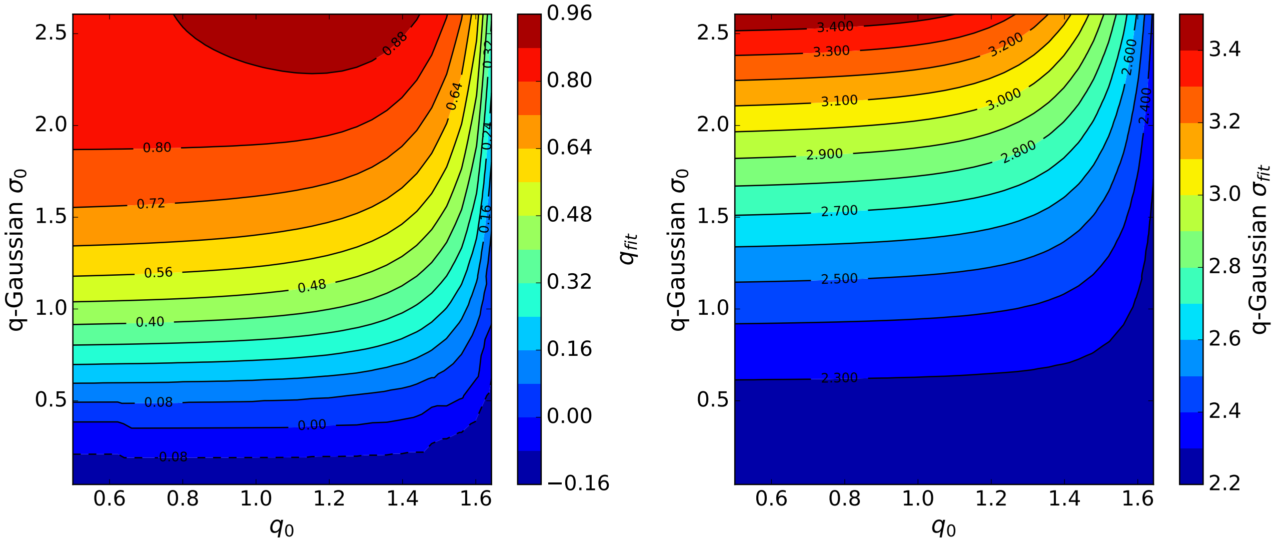

Figure 2.1: Contour plot showing the relationship between q_0 and q-Gaussian σ_0 (corresponding to the betatron distribution) on the x and y axes, and the respective values of q_{fit} and q-Gaussian σ_{fit} from the q-Gaussian fit of the convolution on the z axis.

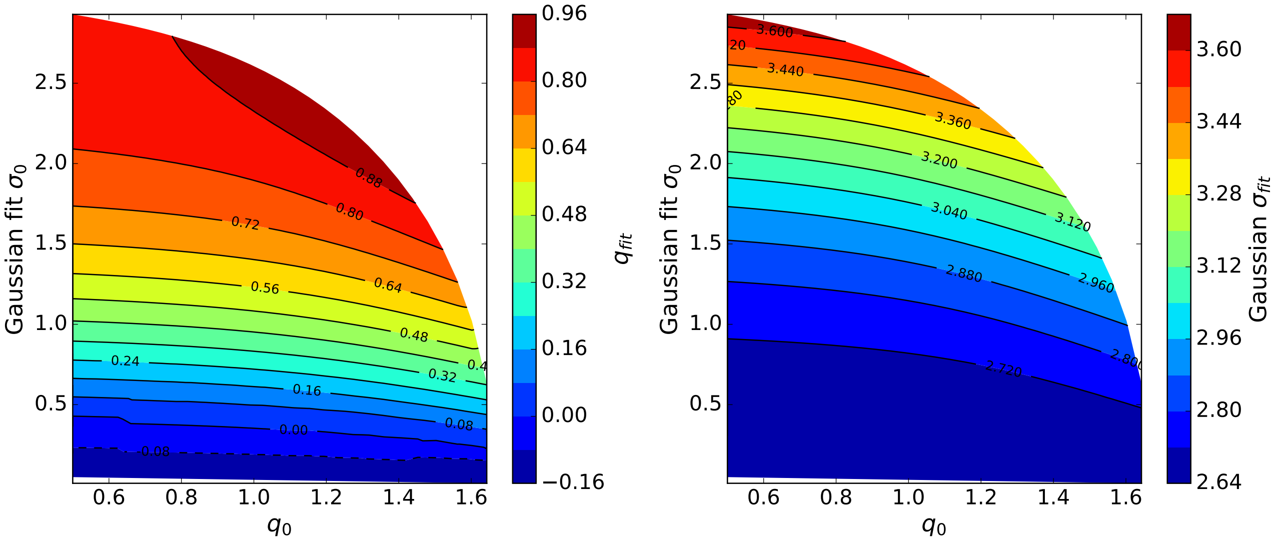

Figure 2.2: Contour plot showing the relationship between q_0 and Gaussian σ_0 (corresponding to the betatron distribution) on the x and y axes, and the respective values of q_{fit} and Gaussian σ_{fit} from the fit of the convolution on the z axis. The Gaussian σ_0 is obtained by fitting the generated q-Gaussian distributions with a Gaussian distribution.

matching simulations, as their effect on specific locations, such as the wire scanner or scraper, is minimal.

In addition to these quadrupoles, the defocusing quadrupoles located in periods 3 and 14 include additional local corrective trims, referred to as $k_{brqd3corr}$ and $k_{brqd14corr}$, respectively.

Moreover, there are four pairs of independently powered quadrupoles, alternating between focusing and defocusing strengths. These are denoted as $k_{br1qno311l1}$, $k_{br1qno412l3}$, $k_{br1qno816l1}$, and $k_{br1qno816l3}$. In each pair, the first quadrupole has a positive strength (focusing), and the second has a negative strength (defocusing). For instance, the quadrupole at position 3l1 has a strength of $+k_{br1qno311l1}$ (focusing), while the quadrupole at position 11l1 has a strength of $-k_{br1qno311l1}$ (defocusing).

Finally, it is important to account for physical constraints. For the $qnos$ series quadrupoles, the

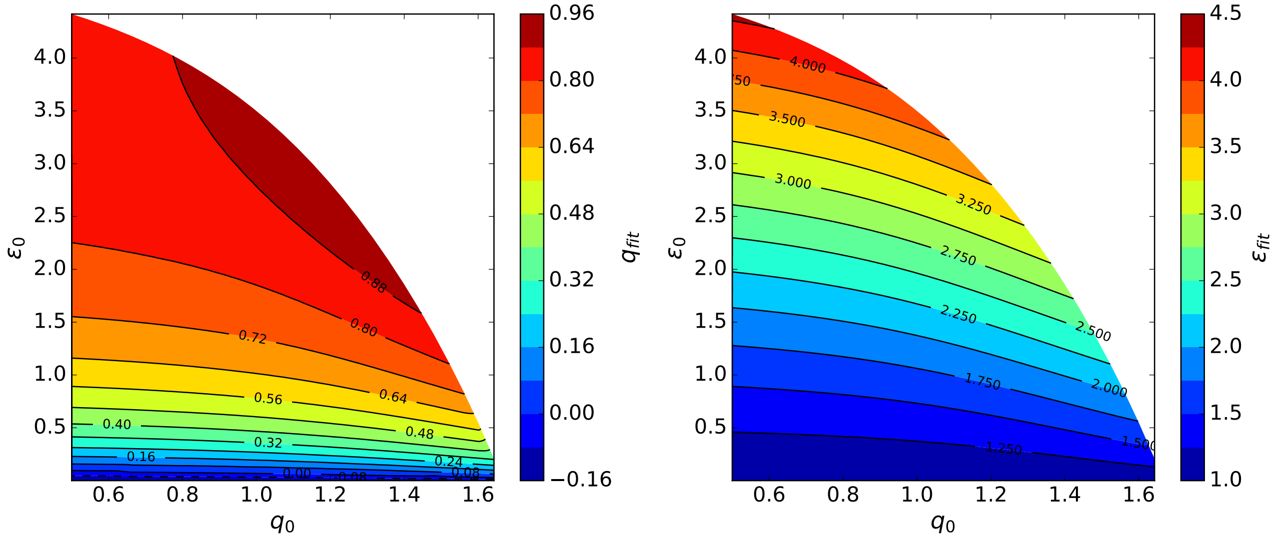

Figure 2.3: Contour plot showing the relationship between the initial transverse distribution parameters q_0 and ε_0 (on the x and y axes) and the corresponding fitted values q_{fit} and ε_{fit} (on the z axis) obtained from the convolution fit. Both ε_0 and ε_{fit} are calculated using the Gaussian sigma, as per its standard definition.

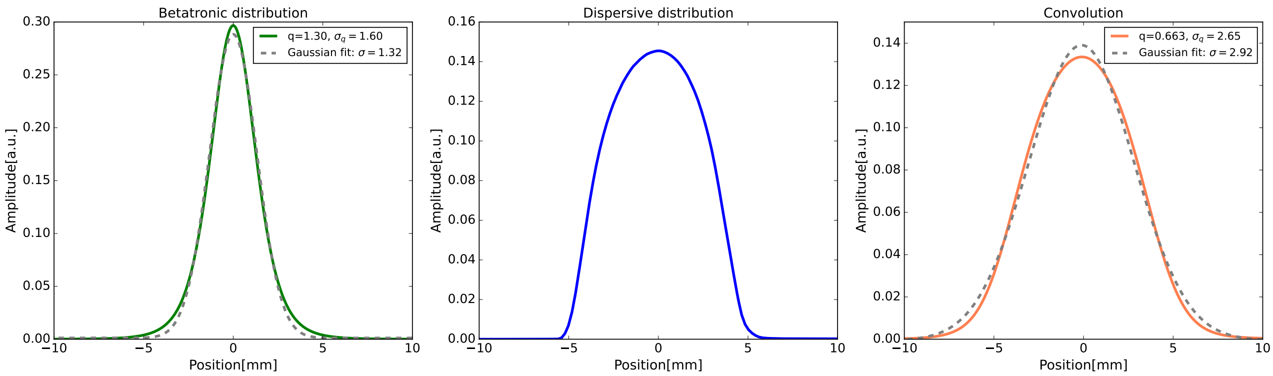

Figure 2.4: In this plot, the green curve represents the q-Gaussian generated with $q = 1.3$ and $\sigma = 1.6$, corresponding to a hypothetical betatronic distribution. The blue curve shows the mean dispersive distribution, and the orange curve is the convolution of the two. The dashed gray line represents the Gaussian fit, with the fit result shown in the label.

maximum current is ±50 A, which corresponds to $-0.015 < k < 0.015$ at flat-bottom energy. The corrective trims are similarly constrained to $-0.025 < k < 0.025$, also at flat-bottom energy.

In the current configuration, the quadrupole at position 3l1, which shares strength with the quadrupole at position 11l1, is disconnected. To implement this configuration, these two quadrupoles have been separated into independent components, designated as $qno3l1$ and $qno11l1$. Since the quadrupole at position 3l1 is disconnected, it is set to $qno3l1 = 0$, with only $qno11l1$ being controlled to reflect the current operating conditions.

Starting from this initial configuration, matching simulations were conducted using *Xsuite* for optical studies such as matching to minimize the dispersion at both the wire scanner and scraper locations, while preserving the horizontal and vertical tune values ($Q_x = 4.17$, $Q_y = 4.23$) at flat-bottom energy. To explore further improvements, an ideal scenario was simulated where the paired quadrupoles could operate fully independently, effectively decoupling their forces. The results of these simulations are presented below, with an analysis of the dispersion D_x and optical parameters β_x and β_y at both locations.

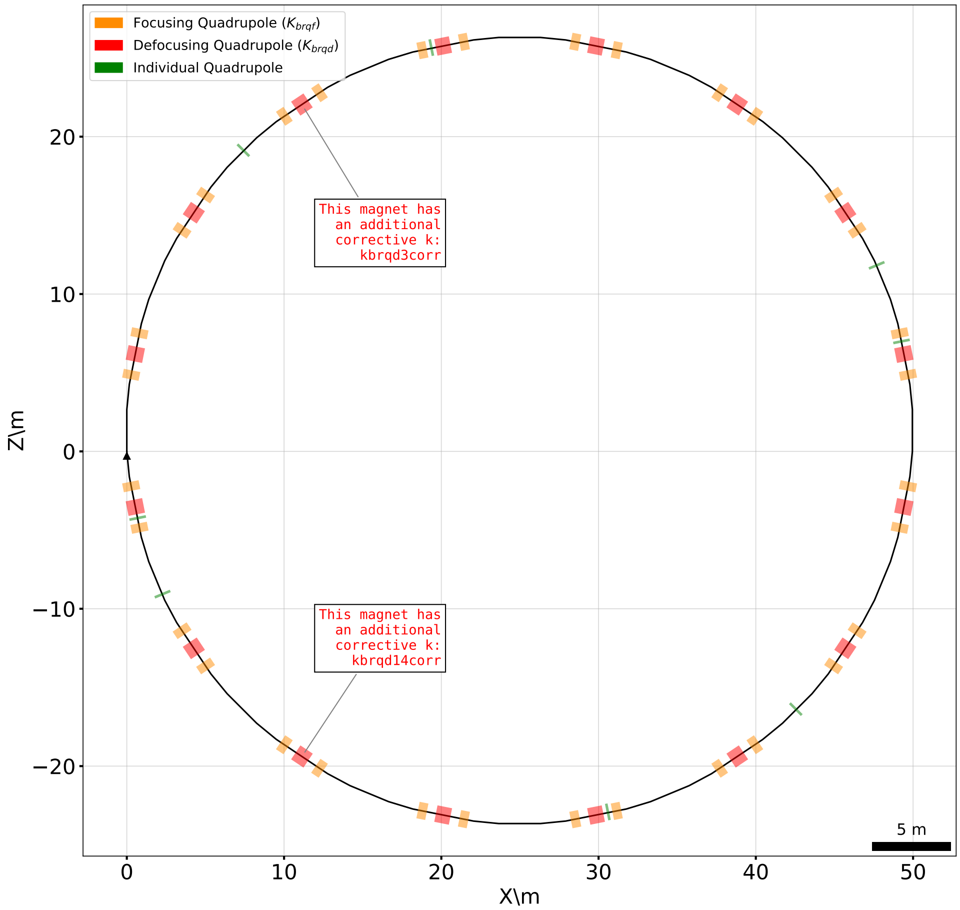

Figure 3.1: Schematic representation of the PSB beamline, highlighting elements relevant for dispersion control. The diagram displays the 16 defocusing quadrupoles (in series), 32 focusing quadrupoles (also in series, with each focusing quadrupole being half the length of a defocusing one), and the individually powered quadrupoles.

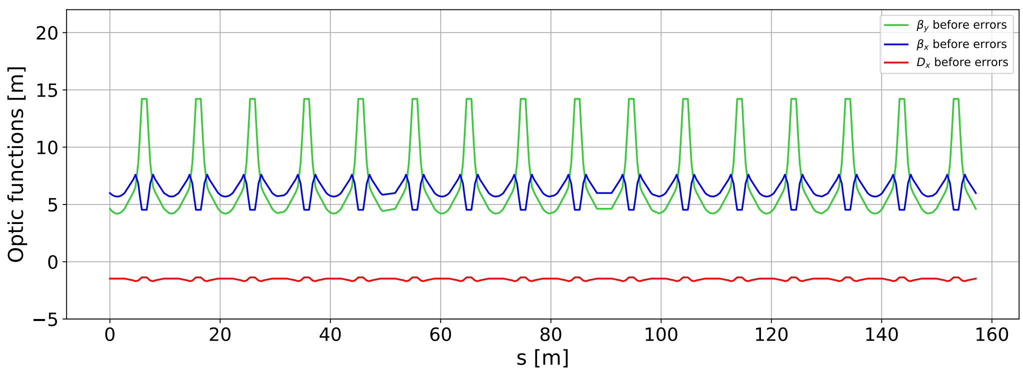

Figure 3.2: Initial configuration of the optical functions along the PSB prior to tune matching. The plot illustrates the distributions of the beta functions, with β_y shown in green, β_x in blue, and the dispersion D_x in red.

3.a Analysis at the wire scanner location

Starting from the initial configuration, the *Match* method in *Xsuite* was used to minimize the horizontal dispersion D_x at the wire scanner location. The optimization process involved

adjusting the strength of the independent quadrupole $qno11l1$, while maintaining the previously established tune values $Q_x = 4.17$ and $Q_y = 4.23$. Additionally, efforts were made to limit beta beating, ensuring that the beta functions remained within acceptable ranges to maintain optimal beam quality.
During optimization, the method iteratively adjusted the strength of the quadrupoles while keeping the β_x and β_y values below the set limits. By the end of the optimization process, a final horizontal dispersion value of $D_x = -1.1755$ m was achieved, reflecting a reduction of approximately 20%. The resulting beta functions at the wire scanner position were measured to be $\beta_x = 5.0861$ m and $\beta_y = 6.4657$ m. The final optical functions as a function of position are shown in Fig.(3.3), which includes the dispersion and beta functions. The plot provides a clear representation of the effectiveness of the matching process.

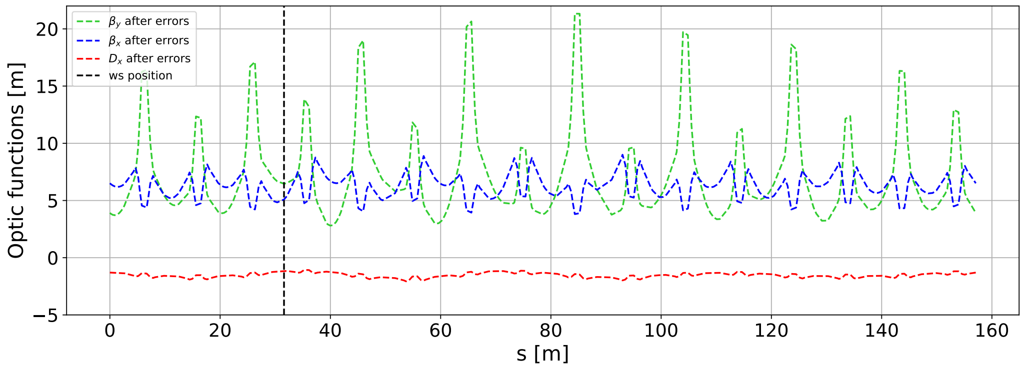

Figure 3.3: Plot showing the main optics functions, starting from the initial configuration, after introducing various errors obtained through matching to minimize D_x at the wire scanner location. The green line represents β_x, the blue line represents β_y, the red line indicates D_x, and the black line marks the position of the wire scanner.

3.b Analysis at the scraper location

For the analysis at the scraper location, the same approach as described for the wire scanner was employed. Utilizing the initial configuration established earlier, the objective was to reduce the horizontal dispersion D_x at the scraper position. Matching simulations for the scraper were conducted, focusing on minimizing the dispersion while preserving the horizontal and vertical tune values and limiting beta beating, similar to the previous steps taken for the wire scanner. At the end of the optimization process, the final value of the horizontal dispersion was $D_x = -1.2046$ m, indicating a reduction of approximately 19%. The beta functions at the scraper position were found to be $\beta_x = 5.5664$ m and $\beta_y = 10.2459$ m. The final optical functions as a function of position are shown in Fig.(3.4), which includes the dispersion and beta functions.

3.c Exploration of other configurations

In addition to the initial configurations analyzed for both the wire scanner and the scraper, the study was extended by systematically repeating the analysis for various hypothetical configurations that could be implemented. This involved separating each of the coupled quadrupoles one by one, thereby exploring the potential for optimizing dispersion in these different configurations.
The results obtained from these analyses are summarized in Tab.(3.1) for the wire scanner and in Tab.(3.2) for the scraper, providing an overview of the dispersion reductions achieved for

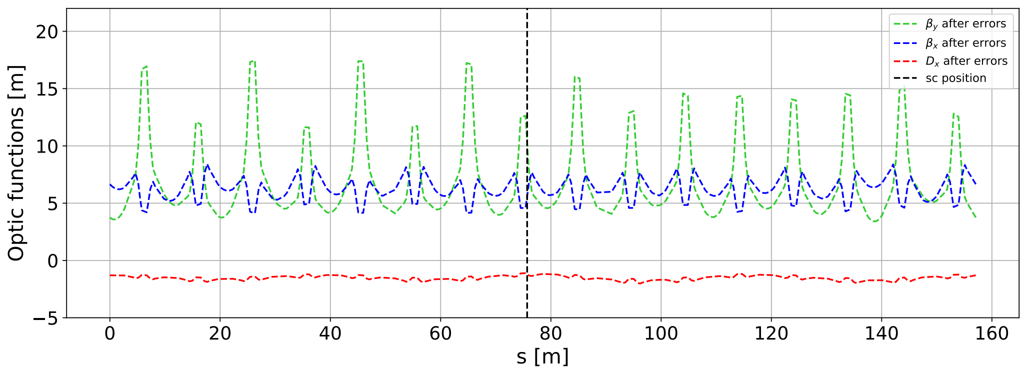

Figure 3.4: Plot showing the main optical functions, starting from the initial configuration, after introducing various errors obtained through matching to minimize D_x at the scraper location. The green line represents β_x, the blue line represents β_y, the red line indicates D_x, and the black line marks the position of the scraper.

each configuration. Furthermore, the results are presented in Fig.(3.5) and (3.6) for both the wire scanner and the scraper. In the first plots, the initial values of β_x and β_y at the considered positions (the wire scanner and scraper, respectively) are shown with dashed lines, along with the final values for the different tested configurations. In the second plots, the beta beating is illustrated, with both the RMS and maximum values reported along the entire line for both x and y. Containing the beta beating is crucial, as excessive beta beating can result in beam loss.

Configuration	$D_x[m]$	$\beta_x[m]$	$\beta_y[m]$	Reduction D_x
Initial without errors	-1.4675	5.8011	4.3614	0%
31111 split	-1.1755	5.0861	6.4657	20%
31111 + 41213 split	1.0980	4.8229	5.7779	25%
31111 + 81611 split	1.0449	5.0137	6.2210	29%
31111 + 81613 split	1.0579	5.2995	5.6183	28%
All split	0.7291	4.5836	6.3134	50%

Table 3.1: Results of the matching simulations for the wire scanner. The table shows the horizontal dispersion D_x and beta functions β_x and β_y for each configuration, along with the percentage reductions of the dispersion from the initial setup.

Configuration	$D_x[m]$	$\beta_x[m]$	$\beta_y[m]$	Reduction D_x
Initial without errors	1.4879	5.5028	11.4829	0%
31111 split	1.2046	5.5664	10.2459	19%
31111 + 41213 split	1.1162	5.4272	10.4815	25%
31111 + 81611 split	1.0671	5.6398	10.6071	28%
31111 + 81613 split	1.1000	5.2973	10.9187	26%
All split	0.7699	5.3067	12.0938	48%

Table 3.2: Results of the matching simulations for the scraper. The table shows the horizontal dispersion D_x and beta functions β_x and β_y for each configuration, along with the percentage reductions of the dispersion from the initial setup.

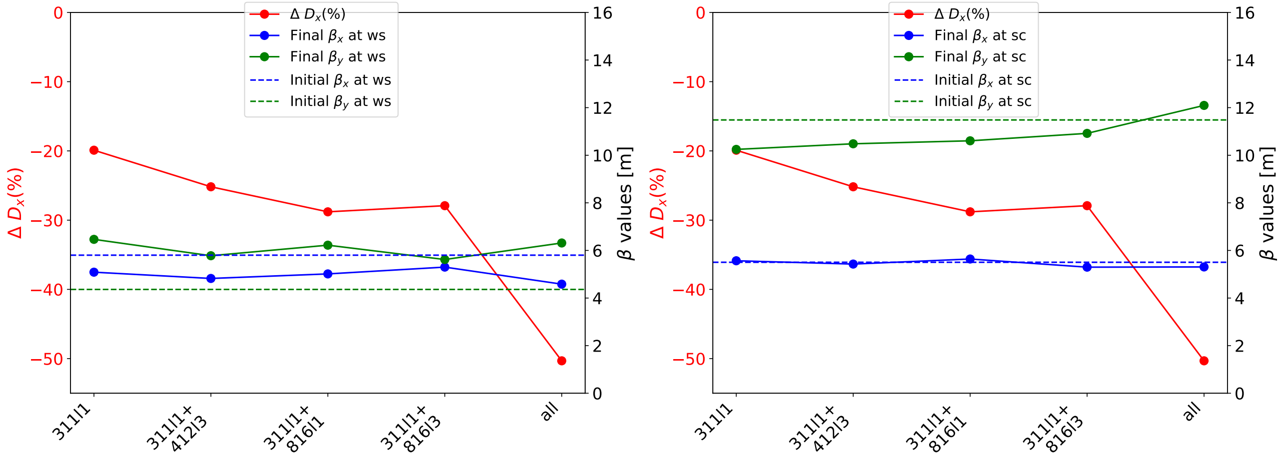

Figure 3.5: These plots summarize the tested configurations aimed at achieving zero dispersion. On the left, the wire scanner results, and on the right, the scraper results. The red line represents the percentage reduction of the final ΔD_x compared to the initial value, while the blue line indicates β_x at the considered position (dashed line shows the initial value) and the green line represents β_y.

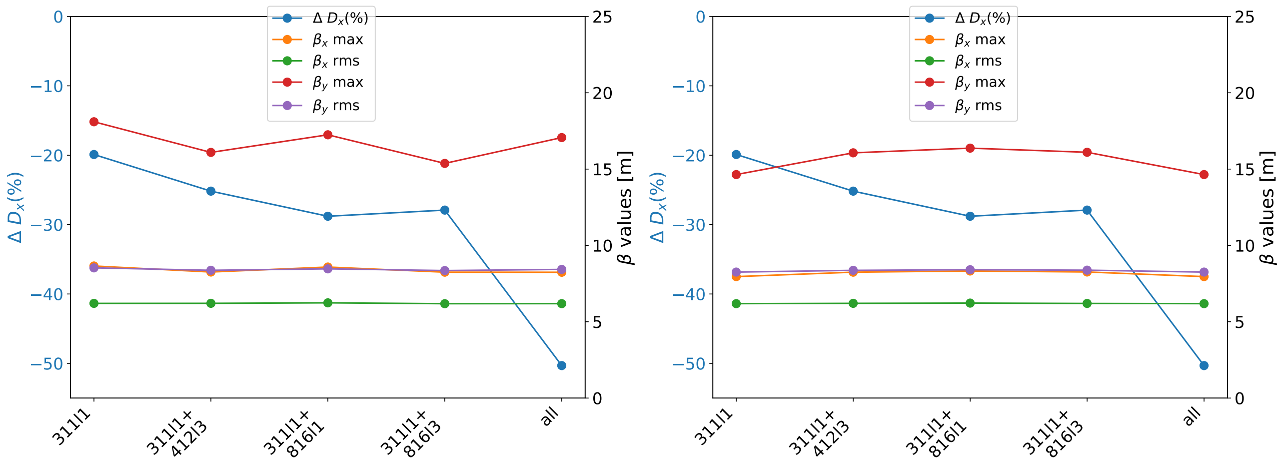

Figure 3.6: This plot illustrates the beta beating that occurs after accounting for errors for the different configurations tested.

4 Measurement of tails emittance at extraction for various $\delta p/p$ values

As discussed earlier, to reduce the contribution of σ_d, action can also be taken on the value of $\delta p/p$. By decreasing $\delta p/p$, σ_d will also be reduced. The next step is to examine how to reduce the momentum dispersion. To this end, the values of the first (H1) and second (H2) harmonics can be adjusted with the aim of reducing the bucket height.

For the acquisition, a clone of the LHC25 standard beam was used. To measure the beam profiles, horizontal and vertical wire scanners were utilized. A wire scanner is a diagnostic tool that moves a thin wire through a particle beam to measure its profile. As the wire intercepts the beam, it interacts with the particles, generating a shower of secondary particles. These secondary particles are detected, producing an amplified current signal that is proportional to the beam's particle density. By scanning the wire across the beam at different positions, the tool provides a precise measurement of the beam's horizontal and vertical dimensions. All

measurements were taken before extraction at 770 ms, during the flat-top phase of the cycle. A very low intensity ($20 \cdot 10^{10}$ ppb) is set across all the booster rings, but attention is focused specifically on ring 3. For five different values of the H1 voltage in the RF cavity: 10 kV (starting value), 9 kV, 7 kV, 5 kV, and 3 kV, tomography is performed. From this tomography, the value of $\delta p/p$ is extracted. Additionally, the horizontal and vertical beam distributions are acquired three times. For the 5 kV and 3 kV settings, the H2 voltage is also reduced to preserve the parabolic shape of the distribution, as shown in Fig.(4.1). The intensity was subsequently increased to $40 \cdot 10^{10}$ ppb, with measurements taken only at 10 kV and 3 kV. Finally, with $60 \cdot 10^{10}$ and $80 \cdot 10^{10}$ ppb, data acquisition was performed exclusively at 3 kV.
The relationship between horizontal emittance and q-values as a function of $\delta p/p$ for the first two intensity levels are illustrated in Fig.(4.2). As $\delta p/p$ decreases, the horizontal emittance also decreases, approaching the value that aligns with the betatron distribution. It is important to note that the dotted line in the graph represents the projection of the fit rather than an actual trend in the data. Additionally, higher intensities generally result in increased emittance values. For q-values, the primary variation observed is in the slope of the fit across different intensities.

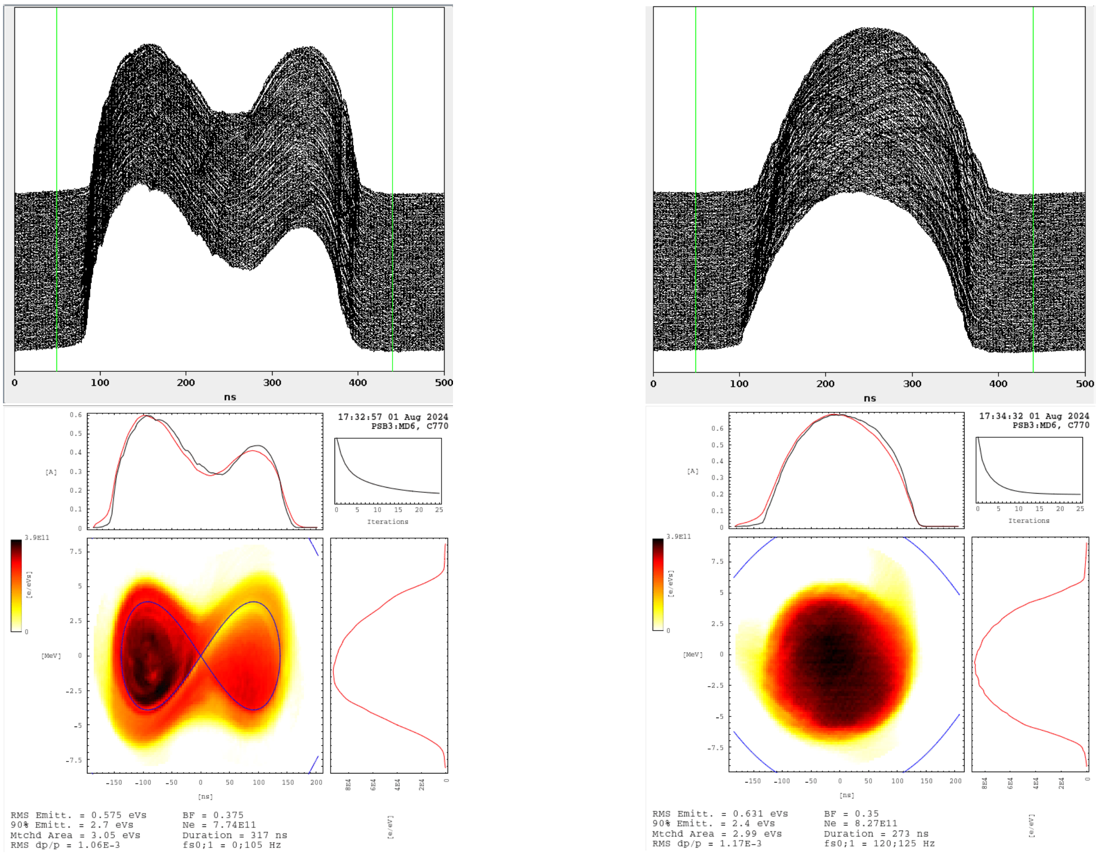

Figure 4.1: The images illustrate how a parabolic distribution can be achieved by adjusting the value of the second harmonic H_2. On the left, the configuration is shown without any modification to H_2, while on the right, the distribution becomes parabolic by reducing the value of the second harmonic.

5 Impact of dispersion on beam brightness

This chapter explores the relationship between brightness, emittance, and q-values, which is crucial for optimizing beam performance.

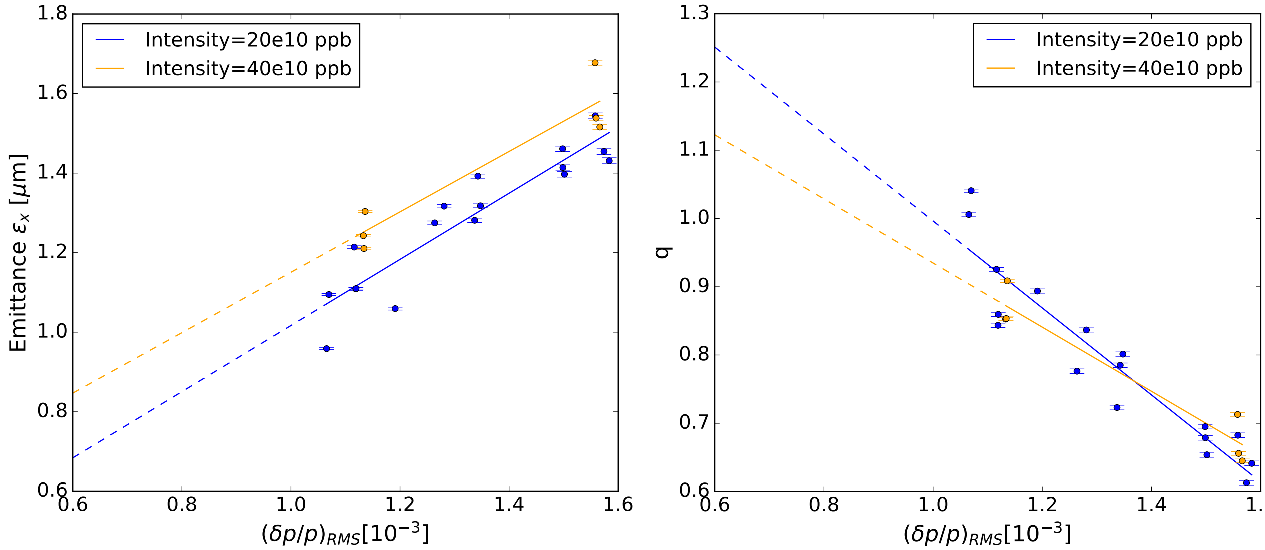

Figure 4.2: The left panel illustrates the horizontal emittance as a function of $\delta p/p$, while the right panel displays the q-values as a function of $\delta p/p$. In the graphs, the blue lines represent the lower intensity ($20 \cdot 10^{10}$ ppb), and the orange lines represent the higher intensity ($40 \cdot 10^{10}$ ppb). Note that the dotted line in each graph represents the projection of the fit rather than an actual trend in the data.

To summarize the measurement process, a series of acquisitions were performed to assess the impact of varying brightness on emittance and q-values. For each intensity level, multiple horizontal and vertical beam profiles were captured and averaged to produce a single data point for analysis. Alongside these profile measurements, the corresponding $\delta p/p$ values for each nominal intensity were recorded, allowing for a better understanding of how these parameters influence beam quality. The obtained graphs are shown in Fig.(5.2), where the dashed lines represent the emittance and q-values corresponding to the vertical plane. The target LIU is indicated by the black dashed line.

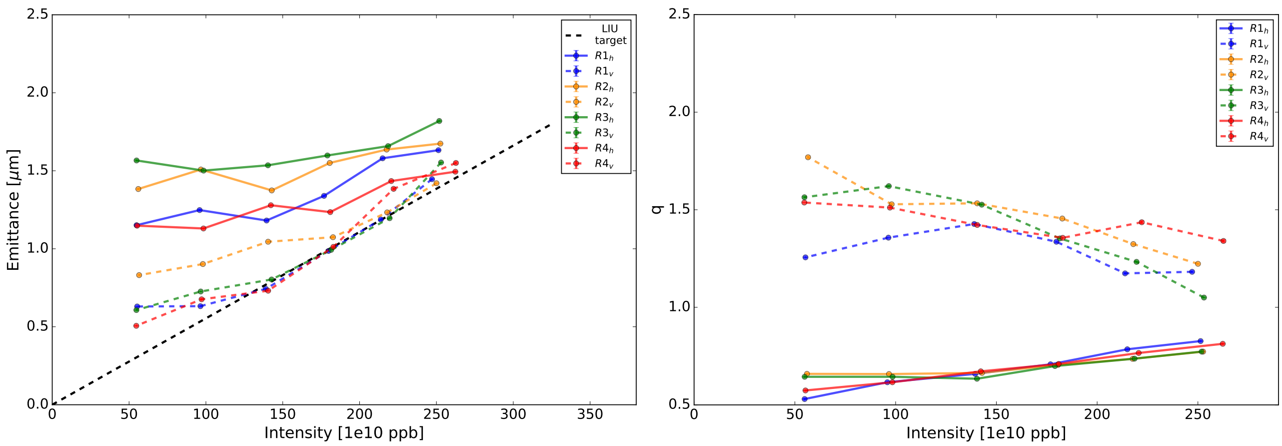

Figure 5.1: On the left, the emittance is plotted as a function of brightness, with a solid line representing the horizontal plane and a dashed line representing the vertical plane. The black dashed line indicates the LIU target. On the right, the same plot is shown, but with q-values replacing emittance.

5.a Repeating measurements with a lower $\delta p/p$ value

The measurements were then repeated in the horizontal plane for reduced $\delta p/p$ values. To achieve this reduction, several adjustments were made: the blow-up effect was removed, and the values of the first harmonic (H1) and second harmonic (H2) were decreased. These changes resulted in a decrease of $\delta p/p$ from an initial value of approximately $1.52 \cdot 10^{-3}$ to a final value of $1.05 \cdot 10^{-3}$. The results obtained are shown in Fig.(**??**), following the same conventions as before.

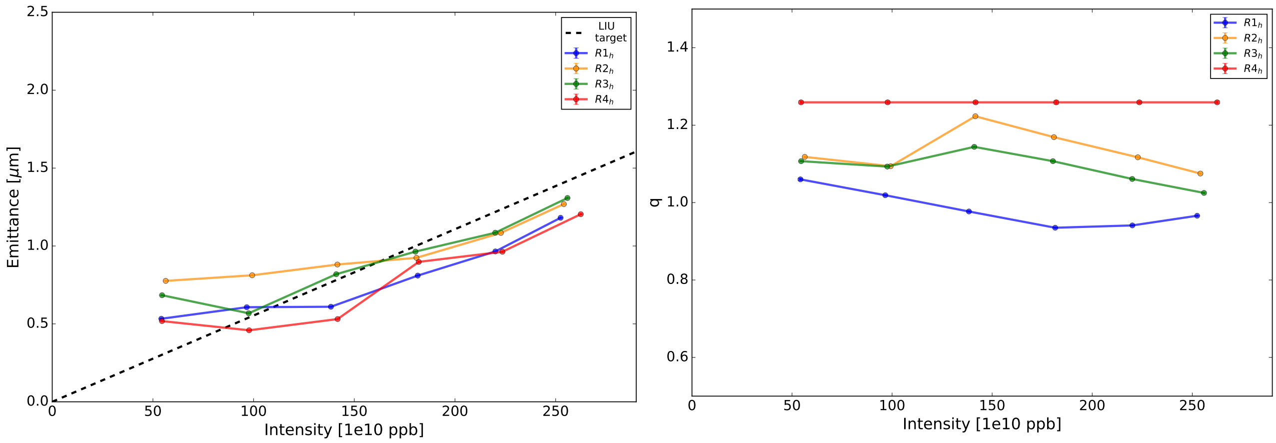

Figure 5.2: On the left, the emittance is plotted as a function of brightness for the the horizontal plane. The black dashed line indicates the LIU target. On the right, the same plot is shown, but with q-values replacing emittance.

6 Conclusion

In this project, the intricate relationship between betatronic distribution and the measured particle beam profiles at the Proton Synchrotron Booster (PSB) was explored. The study revealed the crucial role of dispersion in shaping horizontal beam profiles and led to the development of new methods for extracting key parameters from experimental data. The analysis demonstrated that the beam profiles closely follow q-Gaussian distributions, indicating behavior that extends beyond the standard Gaussian model.

A key discovery was the presence of tails in the horizontal beam profiles, signaling deviations from Gaussian behavior. By modeling the convolution of dispersive and betatronic distributions using q-Gaussian functions, a more accurate understanding of the underlying betatronic dynamics was achieved. Additionally, it was observed that reducing momentum spread is linked to decreased emittance, suggesting potential systematic errors in calculations based on nominal $\delta p/p$ values.

The findings confirmed that the measured brightness achieved the targets set by the LIU project, demonstrating that the PSB is performing as expected. Horizontal dispersion D_x was successfully reduced by up to 20% at critical diagnostic locations, such as the wire scanner and scraper, through careful tuning of the quadrupoles while maintaining the required machine tune. This reduction was achieved only in simulations and was not tested in the actual machine.

In conclusion, this research underscores the importance of controlling dispersion to achieve precise measurements of beam distributions in particle physics experiments. Although complete elimination of dispersion was not possible with the tools used, the results show that its effects can be significantly reduced. Simulations conducted with *Xsuite* provided valuable guidance for optimizing optical elements, particularly quadrupoles, leading to a substantial reduction in horizontal dispersion. Furthermore, the study highlights the complex interdependence of emittance, dispersion, and beam brightness, underscoring the need for a comprehensive understanding of these parameters to maximize beam performance.

A q-Gaussian Distribution

The q-Gaussian is a probability distribution that generalizes the standard Gaussian distribution. The probability density function of a standard q-Gaussian is:

$$f_{QG}(x;q,\beta,\mu) = \frac{\sqrt{\beta}}{C_q} e_q(-\beta(x-\mu)^2) \tag{A.1}$$

where

$$e_q(x) = [1+(1-q)x]_+^{\frac{1}{1-q}} \tag{A.2}$$

is the q-exponential function. The normalization factor C_q is defined as follows:

$$C_q = \begin{cases} \frac{2\sqrt{\pi}\Gamma\left(\frac{1}{1-q}\right)}{(3-q)\sqrt{1-q}\Gamma\left(\frac{3-q}{2(1-q)}\right)} & \text{for } -\infty < q < 1, \\ \sqrt{\pi} & \text{for } q = 1, \\ \frac{\sqrt{\pi}\Gamma\left(\frac{3-q}{2(q-1)}\right)}{\sqrt{q-1}\Gamma\left(\frac{1}{q-1}\right)} & \text{for } 1 < q < 3. \end{cases} \tag{A.3}$$

The parameter q affects the tails of the distribution. As q approaches 1, the q-Gaussian converges to the standard Gaussian distribution. For $1 < q < 3$, the distribution has heavier (more populated) tails compared to the normal distribution. For $q < 1$, the tails are lighter (less populated). For instance, when $q = 0$, the q-Gaussian resembles a parabolic function. Additionally, the normalization factor C_q may require adjustments or a different formulation for proper normalization in this range. The β parameter controls the width of the distribution. Specifically, it affects how quickly the distribution's tails decay. Larger values of β lead to a narrower distribution, while smaller values result in a wider distribution. Typical Q-Gaussian functions for different values of the q and β parameters are shown in figure A.1.
The variance of the q-Gaussian is given by:

$$\sigma_q^2 = \begin{cases} \frac{1}{\beta(5-3q)} & \text{for } q < \frac{5}{3} \\ \infty & \text{for } \frac{5}{3} \le q < 2 \\ \text{Undefined} & \text{for } 2 \le q < 3 \end{cases} \tag{A.4}$$

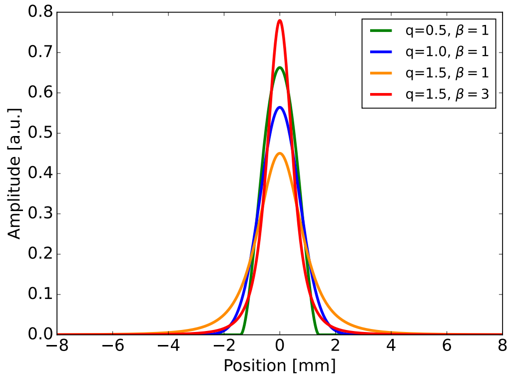

Figure A.1: This plot shows how the shape of the q-Gaussian distribution changes with different values of the parameter q and the scaling parameter β.